

AC Transport at Holographic Quantum Hall Transitions

Janne Alanen,^{1,2*} Esko Keski-Vakkuri,^{1†} Per Kraus,^{3‡} and Ville Suur-Uski^{1,2§}

¹*Helsinki Institute of Physics and ²Department of Physics
P.O.Box 64, FIN-00014 University of Helsinki, Finland*

³*Department of Physics and Astronomy, UCLA, Los Angeles, CA 90095-1547, USA*

Abstract

We compute AC electrical transport at quantum Hall critical points, as modeled by intersecting branes and gauge/gravity duality. We compare our results with a previous field theory computation by Sachdev, and find unexpectedly good agreement. We also give general results for DC Hall and longitudinal conductivities valid for a wide class of quantum Hall transitions, as well as (semi)analytical results for AC quantities in special limits. Our results exhibit a surprising degree of universality; for example, we find that the high frequency behavior, including subleading behavior, is identical for our entire class of theories.

*janne.alanen@helsinki.fi

†esko.keski-vakkuri@helsinki.fi

‡pkraus@ucla.edu

§ville.suur-uski@helsinki.fi

1 Introduction and Summary

Not too long ago, it would have seemed highly unlikely that results from quantum gravity and string theory would find their way into discussions of condensed matter physics. This began to change with an improved understanding of non-perturbative string theory, and especially in the past few years with the steadily growing appreciation of the usefulness of AdS/CFT duality for studying strongly coupled quantum field theories, examples of which abound in condensed matter physics. It is natural to try to forge this connection in systems exhibiting some degree of universality, which has led to a focus on the physics near quantum critical points. The quantum critical point itself is achieved by going to zero temperature and tuning the appropriate coupling constants; however its existence controls the physics in a finite neighborhood transition region that spreads from it. Similarly, the dual gravity theory can have an AdS description that extends to the transition region. The dual description can then be used to study transport at non-zero temperature near the critical point, among other things. This is helpful when it is difficult to perform standard calculations based on traditional models of interacting quasiparticles. For more discussion, see *e.g.* the recent reviews [1, 2, 3].

In this paper we consider AdS dual descriptions of quantum phase transitions corresponding to transitions between different (integer or fractional) quantum Hall plateaus, modeled by a system of intersecting branes [4] (see also [5]). These branes typically have a single mutually transverse direction, and the transition is realized by taking the brane separation to zero, and then continuing through to the other side. We will give analytical results for DC electrical conductivities valid for a wide class of transitions. In the middle of the transition (*i.e.* at the critical point), we will compute the longitudinal and transverse AC conductivities at finite temperature. We will then compare the results to those obtained by Sachdev [6], who studied finite temperature transport near a fractional quantum Hall critical point in a simplified field theoretic toy model proposed by Chen, Fisher and Wu [7]. The model has Dirac fermions coupled to a U(1) Chern-Simons gauge field, converting the fermions to anyons representing the quasiparticles of a fractional quantum Hall state. The system undergoes a quantum transition to an insulator when the mass of the fermions is taken to zero and its sign is reversed, much like what happens in the intersecting brane model.¹

In general, a system undergoing a quantum phase transition has two qualitatively different regimes of charge transport [8, 9], depending on the ratio of the frequency of the current and the temperature, $\hat{\omega} \equiv \hbar\omega/k_B T$: i) collision-dominated low frequency regime $\hat{\omega} \ll 1$, and ii) phase-coherent high frequency regime $\hat{\omega} \gg 1$. In the latter, charge carriers are excited by the external perturbation, and do not collide with

¹In the latter, the transition to zero conductivity is also easily obtained using multiple branes.

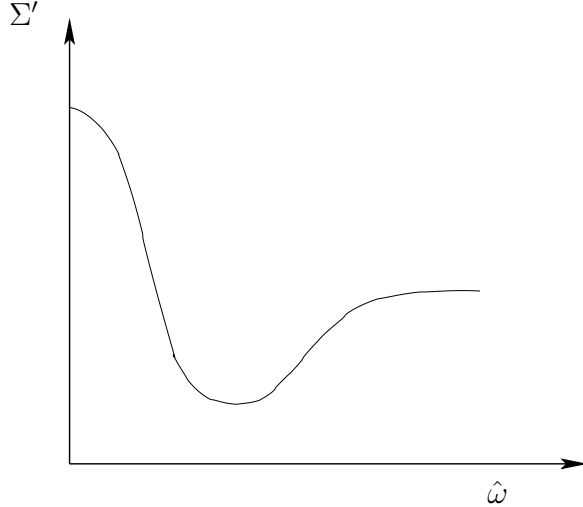


Figure 1: Σ' as a function of $\hat{\omega}$

thermal excitations. A characteristic feature is that at the scale invariant quantum fixed point the dynamic conductivity becomes a universal function of $\hat{\omega}$ [8]. In 2 + 1 dimensions (which we focus on),

$$\sigma(\omega) = \sigma_0 \Sigma(\hat{\omega}) , \quad (1)$$

where σ_0 is the quantum unit of conductance ($\sigma_0 = e_*^2/h$ where e_* is the carrier charge) and $\Sigma(\hat{\omega})$ is the universal function. In the limit $\hat{\omega} \rightarrow \infty$, corresponding either to the high frequency limit $\omega \rightarrow \infty$ at finite T , or the zero temperature limit $T \rightarrow 0$ at finite frequency, the conductivity approaches the universal conductivity $\sigma_0 \Sigma(\infty)$, where $\Sigma(\infty)$ is a pure number, independent of the microscopic details of the system, and can be used to classify quantum critical points. In our dual models this limiting value will be related to an effective brane tension.

The expected characteristic behavior of the real part of the complex valued function Σ , often denoted by Σ' , is sketched in Figure 1 (following [8]). It depicts a Drude peak at small $\hat{\omega}$, and in the collisionless regime $\hat{\omega} \gg 1$ the asymptotic behavior of Σ' is determined by the scale invariance at the critical point. In particular, the conductivity is expected to become temperature independent in the high frequency limit, and then dimensional analysis forces $\Sigma'(\hat{\omega})$ to go to a constant in this limit. In our model, the conductivity at the finite temperature critical point is actually frequency independent; this is the same phenomenon as was observed in [10], and for the same underlying reason. In order to get interesting frequency dependence we further deform the theory by turning on a nonzero charge density and magnetic field. Upon so doing, we will find that the characteristic behavior of the conductivity agrees with the expectation of Fig. 1.

In particular, we will compare our results against those of Sachdev [6], and find unexpectedly good agreement. For the comparison, it is interesting to note that

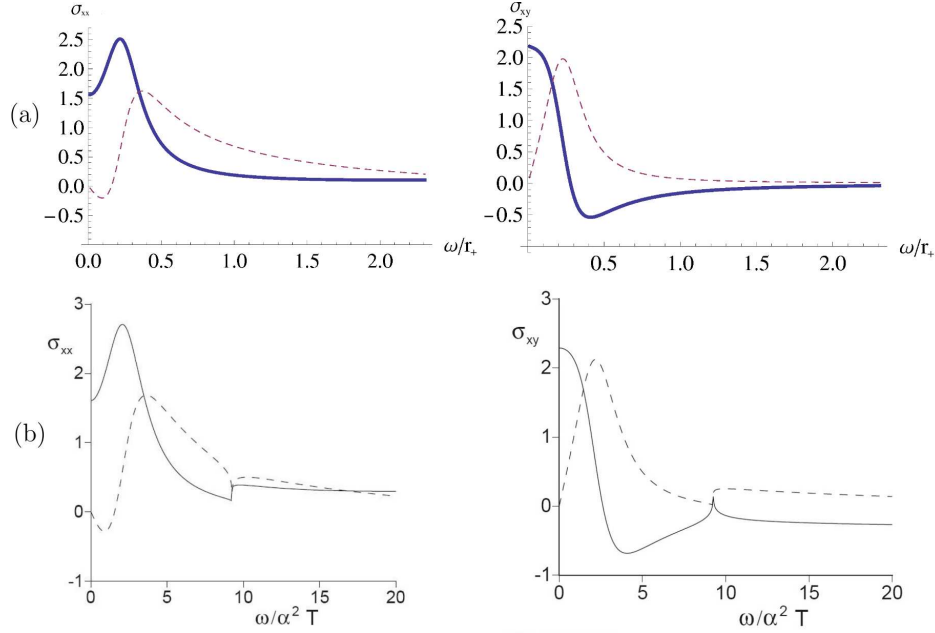


Figure 2: Longitudinal conductivity σ_{xx} and Hall conductivity σ_{xy} a) from the D-brane model and b) from Sachdev's analysis [6]. Real parts are depicted by the solid curves and imaginary parts by the dashed lines. The plots in a) use parameter values $\hat{\rho} = 15.1$, $\hat{B} = 1.4$, $\tau = 0.3$ of the model.

in [6] the results come from various detailed calculations. The Hall conductivity is given entirely by perturbative contributions, reducing to coherent transport of externally created particle-hole pairs, while the longitudinal component also receives a contribution from incoherent collision effects [6]. The analysis is quite tricky even in the simplified model, and some discontinuities remain as artifacts in the final plots of the conductivity. Given the different ingredients that go into the analysis, it is quite remarkable that we find the dual D-brane construction to give such a good match (fitting just two parameters already gives a good fit to the overall shape, and the third parameter fits the asymptotic behavior) to the results of [6]. The comparison is presented in Figures 2 (a) and (b). On the other hand, it should be kept in mind that there are some important differences. Namely, the model studied in [6] is a scale invariant theory, while we are breaking scale invariance by including a nonzero charge density and magnetic field.

As in other AdS setups, numerical methods are needed to compute the AC conductivities for general values of parameters. However, we are also able to find some analytical results in special cases. One case is for the DC conductivity, where we can compute the Hall and longitudinal conductivities during the transition for general values of charge and magnetic fields. Another example is that we can give an almost analytical expression (*i.e.* in terms of an integral) for the AC response at the transition point in the presence of a small charge and magnetic field. We are

not aware of other cases where it is possible to find such a result. We can also give an analytical derivation of the response in the high frequency limit, including the subleading behavior in $1/\omega$. All of these analytical results of course agree with our numerics in the appropriate regime.

Our calculations follow the logic of earlier work on dual models of charge transport, see *e.g.* [10, 11, 12, 13, 14] and the reviews cited above. Studies of the quantum Hall effect in string theory include the early work [15, 16, 17], a recent AdS dual model [18] which utilizes the construction in [19], and the most recent constructions [20, 21] inspired by the ABJM [22] model for M2-brane dynamics.

2 Quantum Hall critical points from intersecting branes

A quantum Hall plateau transition describes a jump in the transverse conductivity σ_{xy} of a 2+1 dimensional system of charged particles as one varies some control parameter. There are a number of different physical mechanisms and control parameters that give rise to this behavior. In the original, experimentally realized, transition, the system consists of electrons subject to disorder, with the control parameter being an external magnetic field. A realization that arises naturally in string theory uses the fact that nonzero transverse conductivities are generated by integrating out massive fermions. In field theory terms, the statement is that one-loop diagrams for charged fermions induce Chern-Simons terms for external gauge fields. Furthermore, the sign of the Chern-Simons terms, and hence the sign of contribution to σ_{xy} , is correlated with the sign of fermion mass (recall that in 2 + 1 dimensions a fermion mass term is *parity odd*.) Thus a plateau transition arises if one (or more) fermion masses is smoothly tuned through zero [23].

Such a situation is achieved in string theory by considering various intersecting brane configurations [4]. If the fermions arise from open strings connecting distinct branes, then the mass is tuned by adjusting the relative separation of the branes in some mutually transverse direction. The external gauge field can be taken to be the gauge fields living on the branes (using a bulk gauge field is also an option in some cases).

Particular interest attaches to the critical theory right at the transition point where some fermions are becoming massless. Geometrically this arises when the intersecting branes coincide, and there is a nontrivial critical theory living on the intersection. To apply gauge/gravity duality in this and other contexts, it is convenient to take the branes carrying the external gauge field (which we'll refer to as the “electromagnetic field”) to be probes living in the near horizon geometry produced by the other branes. This is valid provided that the number of probe branes is small, and indeed we will typically take only a single probe. In the cases of interest the probes live in a geometry

of the form $\text{AdS}_{d+1} \times X$, where at finite temperature the AdS factor is replaced by a black brane solution.

We then look for a family of probe embeddings labeled by a parameter corresponding to the brane separation, or equivalently the fermion mass. Using standard AdS/CFT methods we can compute the conductivities with respect to the electromagnetic field. Here, our main focus is on the critical point itself, achieved when the probe brane extend all the way down AdS into the throat or horizon, and we will compute the AC longitudinal and transverse conductivities of the system.

We now describe two specific realizations of these setups. The impatient reader could skip to section 3, where we summarize the main results and go on to compute electrical transport.

2.1 D3-D7 system

The brane construction [4, 5] contains N_7 D7-branes intersecting N_3 D3-branes over $2+1$ dimensions, summarized by:

$$\begin{array}{cccccccccc} & 0 & 1 & 2 & 3 & 4 & 5 & 6 & 7 & 8 & 9 \\ D3 : & \times & \times & \times & \times & & & & & & \\ D7 : & \times & \times & \times & & \times & \times & \times & \times & \times & \end{array} \quad (2)$$

This intersection has six mixed Neumann-Dirichlet directions, hence it is non-supersymmetric but tachyon free. The massless sector (when the branes coincide in x^9) consists of $N = N_3 N_7$ complex two-component fermions. The model focuses on the $2+1$ dimensional low energy theory of these fermions. They have various interaction terms suppressed by powers of the string scale. With the D3-branes located at $x^9 = 0$ and the D7-branes at $x^9 = L$, the plateau transition arises by smoothly varying L from a negative to positive value, or vice versa.

At strong coupling the system is described by the gravitational dual, which is tractable in the probe approximation [24] $N_7 \ll N_3$. In this limit, for large N_3 and gN_3 , one can treat the D7-branes as probes in the supergravity geometry produced by the D3-branes². The near horizon geometry at finite temperature is

$$ds^2 = \frac{r^2}{R^2}(-h dt^2 + d\vec{x}^2) + \frac{R^2}{r^2}h^{-1}dr^2 + R^2 d\Omega_5^2 \quad (3)$$

with

$$h = 1 - \frac{r_+^4}{r^4} . \quad (4)$$

If we write

$$d\Omega_5^2 = d\psi^2 + \sin^2 \psi d\Omega_4^2 , \quad (5)$$

²See e.g. [25] for a general review on duality constructions with intersecting branes.

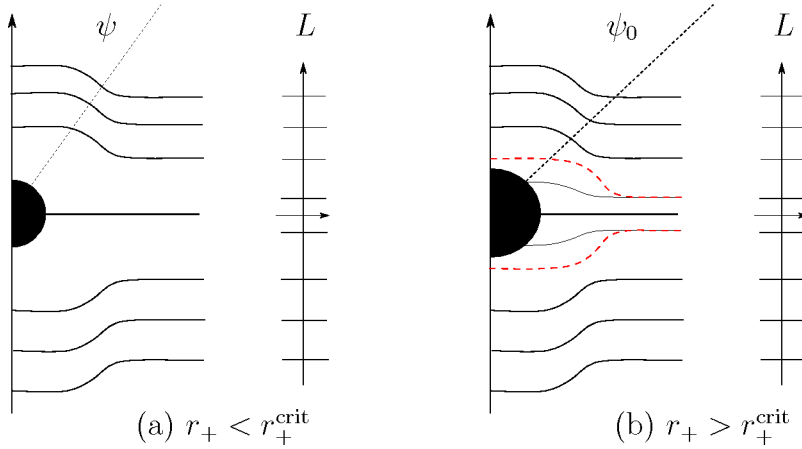


Figure 3: Finite temperature probe embeddings (from [4]). The vertical axis is $x^9 = r \cos \psi$, and the horizontal is $r \sin \psi$. Each embedding asymptotes to some particular x^9 value, $x^9 = L$. The black hole embeddings shown in (b) can also be characterized by the angle ψ_0 at which they enter the horizon. See [4] for discussion of the meaning of r_+^{crit} .

then we can identify the coordinate x^9 in (2) as

$$x^9 = r \cos \psi . \quad (6)$$

The parameters R and r_+ are related to the number of D3-branes and the Hawking temperature by the standard formulas

$$N_3 = \frac{R^4}{4\pi g\alpha'^2} , \quad T = \frac{r_+}{\pi R^2} . \quad (7)$$

The profile of the probe D7-brane is found by solving the equations of motion derived from the Born-Infeld action. The probe lies at some fixed x^3 location, say $x^3 = 0$. At the boundary we impose the boundary condition $x^9 = L$, but then allow x^9 to vary as we move into the bulk; this captures the interactions between the D3 and D7 branes. In the angular coordinates we thus allow for a nontrivial profile $\psi(r)$. At fixed ψ the probe wraps an $S^4 \subset S^5$, and so our full probe geometry wraps an r dependent S^4 . This S^4 either shrinks to zero size at some $r > r_+$, in which case we have a “Minkowski embedding”, or it reaches at finite nonzero size at $r = r_+$, yielding a “black hole embedding”. The different embeddings are sketched in Figure 3.

The probe action consists of two parts: the Born-Infeld action and the Wess-Zumino term which includes the coupling to the background fluxes. The latter contribution will reduce to a Chern-Simons type action, and will be discussed in 2.3. We will first focus on the Born-Infeld action. Starting from the $D = 7 + 1$ dimensional Born-Infeld action and assuming that the worldvolume gauge field has no components tangent to the S^4 , we can integrate over the S^4 to arrive at a $D = 3 + 1$ dimensional

action of the form³

$$S = - \int d^4x \tau(r) \sqrt{-\det(g_4 + F)} . \quad (8)$$

The radius dependent brane tension $\tau(r)$ takes into account the radius dependent size of the wrapped S^4 , and is given by

$$\tau(r) = \frac{N_3 N_7}{3\pi^2} \sin^4 \psi(r) . \quad (9)$$

For the purposes of computing electrical conductivities, it is most convenient to write the induced metric g_4 in terms of Eddington-Finkelstein coordinates, as in [28]. To do so, we need to take into account that the induced metric depends on the profile $\psi(r)$. We can absorb this dependence by defining the new radial coordinate

$$\tilde{r} = \int_{r_+}^r dx \sqrt{1 + h(x)x^2\psi'(x)^2} . \quad (10)$$

The advanced coordinate is then $v = t + r_*$ with $\frac{d\tilde{r}}{dr_*} = \frac{r^2}{R^2}h$. The induced metric takes the form

$$ds^2 = 2dv d\tilde{r} - U(r)dv^2 + \frac{r^2}{R^2}dx^i dx^i \quad (11)$$

with

$$U = \frac{r^2}{R^2}h = \frac{r^2}{R^2} - \frac{r_+^4}{R^2 r^2} , \quad (12)$$

and r understood to be a function of \tilde{r} via (10). The profile function $\psi(r)$, together with the field strength F , can now be computed from (8).

The preceding discussion glossed over one important point. As discussed at length in [4], the $L = 0$ embedding, $\psi = \pi/2$, is unstable, a reflection of the repulsive D3-D7 force. We are going to ignore this issue in the remainder of this paper. One justification is that the instability can be cured by constructions which lead to essentially the same structure; for instance, the next example we discuss, probe D6-branes in the ABJM theory, does not suffer from any instability, but has an effective action of the same basic form as (8). We expect there to be many other such examples.⁴

2.2 D6-branes in ABJM

The ABJM gauge theory [22] is based on a $U(N)_k \times U(N)_{-k}$ Chern-Simons theory with bifundamental matter, and is dual to IIA string theory on $\text{AdS}_4 \times CP^3$. Massless hypermultiplets transforming in the fundamental representation are realized by D6-branes wrapping $\text{AdS}_4 \times RP^3$ [26, 27, 21]. To obtain a Chern-Simons term for the

³we set $2\pi\alpha' = 1$.

⁴The paper [14] introduces an additional flux on the D7-branes; this stabilizes the probe but precludes the possibility of a QHE transition, since it turns out that the probe must always enter the horizon.

D6-brane gauge fields we need to add M units of NS-NS 2-form flux, which shifts one of the gauge group factors to $U(N - M)$, and we also need to give mass m to the hypermultiplets. This results in a Chern-Simons term proportional to M , with a sign correlated with m [21]. Then as above, a plateau transition is realized by a family of massive embeddings that interpolate between opposite sign mass terms.

To be more explicit, the IIA metric is

$$ds^2 = ds_{AdS_4}^2 + 4L^2 ds_{CP^3}^2 \quad (13)$$

where $ds_{AdS_4}^2$ refers to a radius L AdS spacetime (or at finite temperature, a black brane). Writing the metric of CP^3 as

$$ds_{CP^3}^2 = d\xi^2 + \cos^2 \xi \sin^2 \xi (d\psi + \frac{\cos \theta_1}{2} d\phi_1 - \frac{\cos \theta_2}{2} d\phi_2)^2 \quad (14)$$

$$+ \frac{1}{4} \cos^2 \xi (d\theta_1^2 + \sin^2 \theta_1 d\phi_1^2) + \frac{1}{4} \sin^2 \xi (d\theta_2^2 + \sin^2 \theta_2 d\phi_2^2) \quad (15)$$

the massless embedding consists of setting $\xi = \pi/4$, $\theta_1 = \theta_2$, and $\phi_1 = -\phi_2$.

Massive embeddings are obtained by allowing for a nontrivial profile $\xi(r)$, just as in the D3-D7 system above. Taking into account the background fluxes and integrating over the compact space, the resulting Born-Infeld actions is of the same form as in (8) but with

$$\tau(r) = 2\pi k L^6 \sqrt{1 + b^2 \cos^2 2\xi} \sin 2\xi . \quad (16)$$

Here $b = M/(2kL^2)$.

The induced metric takes the form (11) but with

$$U = \frac{r^2}{L^2} h = \frac{r^2}{L^2} - \frac{r_+^3}{L^2 r^3} . \quad (17)$$

and the rescaled radial coordinate is now

$$\tilde{r} = \int_{r_+}^r dx \sqrt{1 + 4(1 + b^2)h(x)x^2 \xi'(x)^2} . \quad (18)$$

To work out the explicit profile $\xi(r)$, and to verify the stability of the massless embedding, we should use the full action, which contains the Wess-Zumino coupling to the RR fluxes in addition to the Born-Infeld term. However, for our computations of AC conductivities we only need the Born-Infeld part.

2.3 Chern-Simons terms

A quantum Hall plateau transition corresponds to a change in the DC Hall conductivity σ_{xy} . From the effective action point of view, this corresponds to a change in the coefficient of the Chern-Simons term for the electromagnetic gauge field. At weak

coupling, when the CFT description is valid, the Chern-Simons term arises from integrating out the massive fermions. At strong coupling, in the gravitational description, Chern-Simons terms arise from an interaction of the probe brane with background fluxes. The corresponding Chern-Simons coefficient depends on the probe embedding, and can change from one quantized value to another as we evolve through a family of embeddings. This is the mechanism used in [4] to describe a plateau transition.

After integrating over the compact space and the radial coordinate, the induced Chern-Simons term in our examples takes the form

$$S_{CS} = \frac{k(\psi_0)}{4\pi} \int A \wedge F , \quad (19)$$

where ψ_0 denotes the angle at which the probe brane enters the horizon (this would be ξ_0 for the ABJM example). As we evolve through a family of embeddings, ψ_0 evolves and induces a transition in $k(\psi_0)$. The Chern-Simons term has the sole effect of contributing to the DC Hall conductivity as $\sigma_{xy} = \frac{k}{2\pi}$. In what follows, we will be computing contributions to the AC conductivity from the Born-Infeld part of the probe action, but we should always remember to add on the Chern-Simons contribution. When we sit right at the critical point of the transition there will be no such contribution since the probe brane embedding is then parity invariant (there could however be a nonzero contribution from other background probe branes with different embeddings).

3 Conductivity for general backgrounds

Based on the two examples discussed in the previous section, we now introduce a general class of models to holographically describe quantum Hall plateau transitions and their critical points. We take the metric

$$ds^2 = 2dvdr - U(r)dv^2 + V(r)dx^i dx^i \quad (20)$$

with $i = 1, 2$. At this stage $U(r)$ and $V(r)$ are general functions compatible with describing an asymptotically AdS_4 black brane metric.⁵ We thus impose

$$U(r), V(r) \sim \frac{r^2}{R^2} \quad \text{as} \quad r \rightarrow \infty . \quad (21)$$

We assume that there is a horizon at $r = r_+$ at which U vanishes linearly in $r - r_+$, and $V(r_+) \neq 0$.

⁵As before, the metric takes the form $ds^2 = 2dvd\tilde{r} - U(r)dv^2 + V(r)dx^i dx^i$, with r understood to be a function of \tilde{r} as in (18). But since in this section we consider arbitrary functions U and V , we can just as well simplify notation and relabel \tilde{r} as r and write the metric as in (20). Asymptotically $\tilde{r} = r$, and so the leading large r behavior shown in (21) is unchanged.

As in the examples, we take the probe action to be a sum of two terms. First, there is the Born-Infeld part with a radius dependent tension⁶

$$S_{BI} = - \int d^4x \tau(r) \sqrt{-\det(g + F)} \quad (22)$$

This radius dependent tension can be thought of as being due to the brane wrapping an r dependent internal space. At $r = \infty$ the tension goes to a constant; we impose this by writing

$$\tau(r) = f(r)\tau_\infty, \quad \lim_{r \rightarrow \infty} f(r) = 1. \quad (23)$$

There is also the Chern-Simons term

$$S_{CS} = \frac{1}{4\pi} \int dk(r) \wedge A \wedge F. \quad (24)$$

The function $f(r)$ arises from the pullback of the bulk fluxes onto the worldvolume. The Chern-Simons level is given by integrating over the radial direction,

$$k = \int_{r_+}^{\infty} dr \partial_r k(r). \quad (25)$$

As described in the previous section, quantum Hall transitions are realized by adjusting the transverse separation L between branes. In the current framework this means adjusting the embedding of the probe, which in turn leads to a one-parameter family of functions τ , U , and V . The parameter L thus controls the transition, in analogy to how an external magnetic field B controls the more familiar plateau transition governed by electronic Landau levels.

Even though we do not need to turn on a magnetic field to describe a transition, it is nonetheless natural to do so, along with a nonzero charge density. As we will see, in the absence of these parameters the conductivities turn out to be independent of frequency, even at finite temperature. With nonzero charge and magnetic field we find a nontrivial frequency dependence, allowing us to compare with the model of [6]. However, it should be kept in mind that these parameters introduce additional length scales into the problem, while in the model of [6] the only scale is set by the temperature.

The gauge field equations of motion following from (22) admit the following solution:

$$F_{12}^{(0)} = B, \quad F_{rv}^{(0)} = \frac{\rho(r)/\tau(r)}{\sqrt{\rho(r)^2/\tau(r)^2 + B^2 + V(r)^2}}. \quad (26)$$

We immediately see that B corresponds to an external magnetic field in the boundary theory. We have also introduced a radial dependent charge density $\rho(r)$, defined by

$$\rho(r) = \frac{\partial \mathcal{L}}{\partial F_{rv}}. \quad (27)$$

⁶Recall that we are setting $2\pi\alpha' = 1$.

The gauge field equations of motion determine the radial dependence as

$$\partial_r \rho(r) = \frac{B}{2\pi} \partial_r k(r) . \quad (28)$$

The standard holographic dictionary identifies the boundary charge density as

$$\rho = \rho(r)|_{r=\infty} . \quad (29)$$

To study the electrical conductivity in linear response we now wish to add a small electric field and compute the resulting current. We consider electric fields and currents that are independent of x^i , but with a general v dependence. We break up the gauge field into a background part plus a small fluctuation:

$$A_\mu = A_\mu^{(0)} + a_\mu , \quad (30)$$

and we'll denote the field strength of a_μ as $f_{\mu\nu}$. The boundary electric field is then

$$E_i(v) = \lim_{r \rightarrow \infty} f_{vi} . \quad (31)$$

Note that v plays the role of time on the boundary.

As with the charge density, we introduce a radius dependent current as

$$j^i(v, r) = \frac{\partial \mathcal{L}}{\partial f_{ri}} , \quad (32)$$

whose radial dependence is given by the a_i equation of motion,

$$\partial_r j^i(v, r) = \frac{1}{2\pi} \partial_r k(r) \epsilon_{ij} E_j . \quad (33)$$

The boundary current is then computed as

$$j^i(v) = j^i(v, r)|_{r=\infty} . \quad (34)$$

Given our assumptions about the asymptotic form of the metric, this works out to be

$$j^i(v) = \lim_{r \rightarrow \infty} \left(\frac{r^2}{R^2} f_{ri} + f_{vi} \right) \tau_\infty . \quad (35)$$

The entries of the conductivity tensor are defined by

$$j^i = \sigma_{ij} E^j . \quad (36)$$

Due to rotational invariance we have $\sigma_{xx} = \sigma_{yy}$ and $\sigma_{xy} = -\sigma_{yx}$. To compute σ_{ij} we need to solve the gauge field equations of motion, subject to the boundary condition (31), and then compute the current from (35). In doing so, it is also crucial to impose smoothness of the solution at the horizon $r = r_+$. Eddington-Finkelstein coordinates cover the future horizon but not the past horizon, so our smoothness condition is

really a statement about the behavior of the solution at the future horizon only. This condition is equivalent, but more general, than the condition [29] of imposing “ingoing boundary conditions” at the horizon. It is more general since it extends beyond linear response [28], though this advantage will not be relevant here.

Since we are describing linear response, we only need the action for quadratic fluctuations of the gauge fields. The Born-Infeld part is

$$S = \frac{1}{2} \int d^4x \frac{\tau(r)}{\sqrt{\Delta_0}} \left[2V f_{ri} f_{vi} - 2BF_{rv}^{(0)} \epsilon_{ij} f_{vi} f_{rj} + UV f_{ri} f_{ri} \right] \quad (37)$$

with

$$\Delta_0 = (B^2 + V^2)(1 - (F_{rv}^0)^2) = \frac{(B^2 + V^2)^2}{\rho(r)^2/\tau(r)^2 + B^2 + V^2} . \quad (38)$$

The Chern-Simons part is

$$S_{CS} = -\frac{1}{4\pi} \int d^4x \partial_r k(r) \epsilon_{ij} a_i f_{vj} . \quad (39)$$

The nontrivial Maxwell equations take the form

$$\partial_r \left[\left(\mathcal{A}(r) \delta_{ij} + \mathcal{B}(r) \epsilon_{ij} \right) f_{vi} + \mathcal{C}(r) f_{ri} \right] + \partial_v \left[\left(\mathcal{A}(r) \delta_{ij} - \mathcal{B}(r) \epsilon_{ij} \right) f_{rj} \right] = -\frac{k'(r)}{2\pi\tau_\infty} \epsilon_{ij} f_{vj} \quad (40)$$

with

$$\mathcal{A} = \frac{f(r)V}{\sqrt{\Delta_0}} , \quad \mathcal{B} = \frac{f(r)F_{rv}^{(0)}B}{\sqrt{\Delta_0}} , \quad \mathcal{C} = \frac{f(r)UV}{\sqrt{\Delta_0}} . \quad (41)$$

Under our assumptions the large r behavior of these functions is

$$\mathcal{A} \sim 1 , \quad \mathcal{B} \sim 0 , \quad \mathcal{C} \sim \frac{r^2}{R^2} . \quad (42)$$

Choosing the gauge $a_r = 0$ the equations of motion become

$$\mathcal{C} \partial_r^2 a_i + (2\mathcal{A} \partial_v + \mathcal{C}') \partial_r a_i + (\mathcal{A}' \delta_{ij} + \mathcal{B}' \epsilon_{ij}) \partial_v a_j = -\frac{k'(r)}{2\pi\tau_\infty} \epsilon_{ij} \partial_v a_j . \quad (43)$$

Next, we give the components (a_v, a_i) a harmonic time dependence $e^{-i\omega v}$, and form the complex combinations

$$a_\pm = a_x \pm i a_y , \quad (44)$$

leading to

$$\mathcal{C} \partial_r^2 a_\pm + (\mathcal{C}' - 2i\omega\mathcal{A}) \partial_r a_\pm - i\omega(\mathcal{A}' \mp i\mathcal{B}') a_\pm = \pm \frac{k'(r)}{2\pi\tau_\infty} \omega a_\pm . \quad (45)$$

Asymptotically AdS solutions will have asymptotic behavior

$$a_\pm = a_\pm^{(0)} + \frac{R^2}{r} a_\pm^{(1)} + \dots \quad (46)$$

This gives an electric field and current

$$E_\pm = f_{v\pm} = -i\omega a_\pm^{(0)} , \quad j_\pm = \tau_\infty(-a_\pm^{(1)} - i\omega a_\pm^{(0)}) . \quad (47)$$

The conductivities are therefore

$$\sigma_\pm(\omega) = \left(1 - i\frac{a_\pm^{(1)}}{\omega a_\pm^{(0)}}\right) \tau_\infty . \quad (48)$$

In xy coordinates we have

$$\sigma_{xx} = \sigma_{yy} = \frac{1}{2}(\sigma_+ + \sigma_-) , \quad \sigma_{xy} = -\sigma_{yx} = \frac{i}{2}(\sigma_+ - \sigma_-) . \quad (49)$$

What we've computed above is the contribution to the conductivity from the Born-Infeld part of the probe action. As discussed in section (2.3), in general we should also add in the contribution from the Chern-Simons term on the probe, which shifts the DC Hall conductivity by the amount $\sigma_{xy} = \frac{k}{2\pi}$.

Computation of the AC conductivity has now been reduced to solving (45). In general, this requires numerical analysis and specific choices for the functions τ , U , and V . In particular limits we can solve the problem analytically, as we discuss in the next few sections. In the following we will always be assuming that the probe is described by a black hole embedding; this is necessary in order for the dissipative part of the conductivity to be nonzero, since for a Minkowski embedding there is nowhere for energy to flow out of the system (at least in the probe approximation).

3.1 DC limit

First consider the $\omega \rightarrow 0$ DC limit. In this limit we can compute the conductivities in the general case. This includes the DC conductivity at and away from the critical point for our entire class of theories. A similar computation was given in [30]. Looking at (48), we see that to compute the DC conductivity we need to compute a_\pm to first order in ω .

At zeroth order the equation of motion (45) becomes

$$\partial_r(\mathcal{C}\partial_r a_\pm) = 0 . \quad (50)$$

Assuming there is a horizon where U vanishes linearly in $r - r_+$, the only smooth solution is $a_\pm = c_\pm$, a constant. Plugging this in, we have at the next order the equation

$$\partial_r(\mathcal{C}\partial_r a_\pm) = i\omega\partial_r(\mathcal{A} \mp i\mathcal{B} \mp i\frac{k(r)}{2\pi\tau_\infty})c_\pm \quad (51)$$

the smooth solution to which is

$$\partial_r a_\pm(r) = \frac{i\omega}{\mathcal{C}(r)} \left[\left(\mathcal{A}(r) \mp i\mathcal{B}(r) \pm i\frac{k(r)}{2\pi\tau_\infty} \right) - \left(\mathcal{A}(r_+) \mp i\mathcal{B}(r_+) \mp i\frac{k(r_+)}{2\pi\tau_\infty} \right) \right] c_\pm . \quad (52)$$

This has large r behavior

$$\partial_r a_{\pm}(r) \sim \frac{i\omega R^2}{r^2} \left[1 - (\mathcal{A}(r_+) \mp i\mathcal{B}(r_+)) \mp i\frac{k}{2\pi\tau_{\infty}} \right] c_{\pm} \quad (53)$$

and so we read off

$$a_{\pm}^{(1)} = -i\omega \left[1 - (\mathcal{A}(r_+) \mp i\mathcal{B}(r_+)) \mp i\frac{k}{2\pi\tau_{\infty}} \right] c_{\pm} . \quad (54)$$

Using that $a_{\pm}^{(0)} = c_{\pm} + \mathcal{O}(\omega)$, we find the DC conductivity

$$\sigma_{\pm} = \left(\mathcal{A}(r_+) \mp i\mathcal{B}(r_+) \right) \tau_{\infty} \mp i\frac{k}{2\pi} , \quad (55)$$

or,

$$\begin{aligned} \sigma_{xx} = \sigma_{yy} &= \mathcal{A}(r_+) \tau_{\infty} = \frac{\sqrt{\rho(r_+)^2/\tau(r_+)^2 + B^2 + V(r_+)^2}}{B^2 + V(r_+)^2} V(r_+) \tau(r_+) \\ \sigma_{xy} = -\sigma_{yx} &= \mathcal{B}(r_+) \tau_{\infty} = \frac{\rho(r_+) B}{B^2 + V(r_+)^2} + \frac{k(\psi_0)}{2\pi} . \end{aligned} \quad (56)$$

In the last line we have indicated that the Chern-Simons level k depends on the angle ψ_0 at which the probe enters the horizon. From (28) the quantity $\rho(r_+)$ is related to the actual charge density as

$$\rho(r_+) = \rho - \frac{kB}{2\pi} . \quad (57)$$

Taking $k = 0$ we can check that our result agrees with that in [30].

The result (56) has some interesting features. First, the conductivities are independent of the metric function U . In fact, the only dependence on the original black brane metric is through $V(r_+)$, which is a measure of the entropy density of the black brane. In particular, for a probe embedded in an asymptotically $d+1$ dimensional black brane geometry, the entropy density is proportional to $(V(r_+))^{\frac{d-1}{2}}$. The only other theory dependent parameter is the brane tension at the horizon, $\tau(r_+)$. So we see that the DC conductivities are nearly universal functions of ρ , B and the entropy density, with only one additional parameter, $\tau(r_+)$. This is an interesting holographic prediction for a large class of critical points.

One interesting special case is $\tau(r_+) = 0$, which gives

$$\begin{aligned} \sigma_{xx} = \sigma_{yy} &= \frac{\rho V(r_+)}{B^2 + V(r_+)^2} \\ \sigma_{xy} = -\sigma_{yx} &= \frac{\rho B}{B^2 + V(r_+)^2} \end{aligned} \quad (58)$$

This value of $\tau(r_+)$ corresponds to a critical embedding which just touches the horizon. It can be thought of as the special case for which the black hole and Minkowski family of embeddings meet. It represents a metal-insulator transition, as can be seen from the fact that the conductivity vanishes in the absence of a net charge density. What is interesting is that the conductivities here are universal functions of ρ , B , and the entropy density.

3.2 Small (B, ρ) expansion at the critical point

At $B = \rho = 0$ the AC conductivity turns out to be independent of ω as a consequence of electric-magnetic duality in the bulk [13]. For general (B, ρ) we require numerical analysis to determine the ω dependence. It is useful to consider an expansion to first nontrivial order in (B, ρ) in order to obtain an analytical expression with a nontrivial ω dependence. To make analytical progress we will also assume that we are at the critical point of the transition, which implies that $f(r) = 1$, and hence constant τ ; recall that this means that the probe is then wrapping a fixed internal space, not depending on r . Also, recall that the Chern-Simons term is absent at the critical point.

Setting $B = \rho = 0$ in (45) the solution for a_{\pm} is simply a constant. Since the conductivity (48) is independent of the overall normalization of a_{\pm} , we can choose $a_{\pm} = 1$ at this order, and also impose this value as a boundary condition at the horizon at every order in ω .

At the next order we write

$$a_{\pm} = 1 + b_{\pm} , \quad (59)$$

with the boundary condition $b_{\pm}(r_+) = 0$ as explained above. We expand in the parameter $\epsilon \sim (B, \rho)$, and we readily find $b_{\pm} \sim \epsilon^2$. The expansions for the coefficient functions are

$$\begin{aligned} \mathcal{A} &= f(r) \left[1 + \frac{1}{2V(r)^2} (\tilde{\rho}^2 - B^2) \right] + \dots \\ \mathcal{A}' \mp i\mathcal{B}' &= f'(r) - \frac{f'(r)}{2V(r)^2} (\tilde{\rho}^2 + B^2) + \frac{f(r)V'(r)}{V(r)^3} (B \pm i\tilde{\rho})^2 + \dots , \end{aligned} \quad (60)$$

where we are writing $\tilde{\rho} = \rho/\tau$. Substituting in, we find that at this order b_{\pm} obeys the equation

$$(Ub'_{\pm} - 2i\omega b_{\pm})' = -\frac{i\omega}{2} (B \pm i\tilde{\rho})^2 \left(\frac{1}{V^2} \right)' . \quad (61)$$

We integrate twice to get

$$b_{\pm}(r) = \frac{i\omega}{2} (B \pm i\tilde{\rho})^2 \int_{r_+}^r \frac{dx}{U(x)} \left(\frac{1}{V(r_+)^2} - \frac{1}{V(x)^2} \right) e^{2i\omega \int_x^r \frac{dy}{U(y)}} , \quad (62)$$

where we imposed the boundary condition $b_{\pm}(r_+) = 0$.

From this we can read off the asymptotic behavior of the full solution to the required order:

$$a_{\pm}(r) = 1 + b_{\pm}(\infty) - 2i\omega \left(b_{\pm}(\infty) + \frac{(B \pm i\tilde{\rho})^2}{4V(r_+)^2} \right) \frac{R^2}{r} + \dots \quad (63)$$

This finally gives the AC conductivity to order ϵ^2 :

$$\sigma_{\pm}(\omega) = \tau - \frac{\tau}{2} (B \pm i\rho/\tau)^2 G(\omega) \quad (64)$$

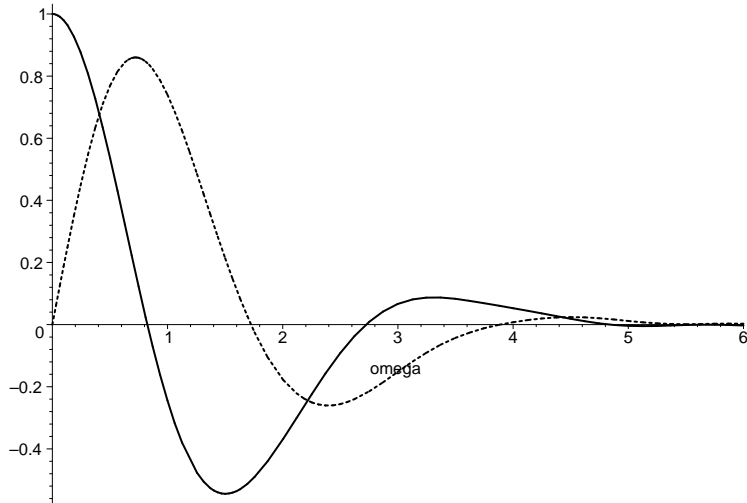


Figure 4: The real (solid) and imaginary (dashed) parts of $G(\omega)$. Note the resemblance of the real part to Fig. 1.

with

$$G(\omega) = \frac{1}{V(r_+)^2} + 2i\omega \int_{r_+}^{\infty} \frac{dx}{U(x)} \left(\frac{1}{V(r_+)^2} - \frac{1}{V(x)^2} \right) e^{2i\omega \int_x^{\infty} \frac{dy}{U(y)}}. \quad (65)$$

Equivalently:

$$\begin{aligned} \sigma_{xx}(\omega) &= \tau + \frac{1}{2}\tau(\rho^2/\tau^2 - B^2)G(\omega) \\ \sigma_{xy}(\omega) &= \rho B G(\omega), \end{aligned} \quad (66)$$

Let us comment on the regime of validity of this result. In solving the differential equation we kept terms of order $\omega\epsilon^2$ and discarded terms of order $\omega^2\epsilon^4$. Thus we actually need $\omega\epsilon^2$ to be small, and not just ϵ itself. Hence, for fixed small (B, ρ) the result is valid for large, but not arbitrarily large, frequencies.

Above we show a plot (Fig. 4) of the real and imaginary parts of $G(\omega)$ in the case corresponding to the D3-D7 system (and setting $r_+ = R = 1$ by a rescaling), for which $U = r^2 - \frac{1}{r^2}$ and $V = r^2$.

For small (B, ρ) this leads to excellent agreement with our general numerical results. We see that $G(\omega)$ exhibits oscillations on a scale set by the temperature,

$$\Delta\omega \sim r_+ \sim T.$$

3.3 High frequency limit and universal conductivity

We now turn our attention to the high-frequency limit $\omega/T \gg 1$ of the conductivity. We first make some general comments to put our results in context. A condensed matter system at a quantum critical point is described at large spacetime length scales by a scale invariant quantum field theory [31]. Within this regime, finite temperature can be introduced into the quantum field theory, as can additional large length scales corresponding to magnetic fields and charge densities. One thus has a finite temperature scale invariant QFT deformed by various operators and charge densities, which is the description that AdS/CFT seeks to make contact with.

If we sit right at the fixed point but turn on finite temperature, the AC conductivity can only be a function of ω/T . As discussed in, *e.g.*, [8] the functional dependence on ω/T is universal in this regime, with any non-universality suppressed by powers of microscopic length scales. It follows that large ω is equivalent to small T , and that the conductivity in the limit $\omega/T \rightarrow \infty$ defines a universal number in dimensionless units. This number is to be distinguished from the DC conductivity at the transition, which is defined by the limit $\omega/T \rightarrow 0$.

Similarly, we can compute or measure the limiting values of the conductivity in the presence of nonzero magnetic fields and charge densities. These describe relevant deformations of the theory, and so are expected to have an important affect at low frequencies but not at high frequencies.

We can make these points precise. We already computed the general DC conductivity in (55). As seen from (56), it is purely a function of quantities evaluated at the horizon, which accords with general intuition on the relation between AdS radial position and boundary length scales. The conductivity in the limit $\omega/T \rightarrow \infty$ is also easily computed. Examining (45) we see that a_{\pm} is a well defined solution in the limit, and then from (48) we have that

$$\lim_{\omega/T \rightarrow \infty} \sigma_{\pm}(\omega/T) = \tau_{\infty} . \quad (67)$$

So in the limit the conductivity is determined purely by the asymptotic brane tension. Note that this result holds at nonzero (B, ρ) , confirming the intuition that these are relevant deformations, and hence unimportant in the UV.

It is also interesting to discuss the subleading behavior as $\omega/T \rightarrow \infty$. Interestingly, this can be determined explicitly for our general class of models at the critical point. We will take $R = 1$ by rescaling r to simplify some expressions. We proceed by solving the differential equation (45) as a power series in $1/\omega$. We write

$$\hat{a}_{\pm} = b_0 + \frac{b_1}{\omega} + \frac{b_2}{\omega^2} + \dots \quad (68)$$

At lowest order we find

$$b_0(r) = \frac{c_0}{\sqrt{\mathcal{A}(r)}} e^{\pm \frac{i}{2} \int_{r_+}^r d\tilde{r} \frac{\mathcal{B}'(\tilde{r})}{\mathcal{A}(\tilde{r})}}. \quad (69)$$

The integration constant c_0 can be chosen arbitrarily since it cancels out of the conductivity. We choose it so that $b_0(\infty) = 1$.

Substituting in the expansion (68) into (45), we obtain the recursion relation

$$2\mathcal{A}b'_{n+1} + (\mathcal{A}' \mp i\mathcal{B}')b_{n+1} = -i(\mathcal{C}b'_n)', \quad (70)$$

which we solve as

$$b_{n+1}(r) = -\frac{i}{2\sqrt{\mathcal{A}(r)}} \int_{r_+}^r d\tilde{r} \frac{\mathcal{C}(\tilde{r})b'_n(\tilde{r})}{\sqrt{\mathcal{A}(\tilde{r})}} e^{\mp \frac{i}{2} \int_{\tilde{r}}^r d\hat{r} \frac{\mathcal{B}'(\hat{r})}{\mathcal{A}(\hat{r})}}. \quad (71)$$

The free integration constant can again be chosen at will, since it can be absorbed into c_0 . From the formula (48) for the conductivity, we know that a subleading contribution at large frequency arises from a nonzero $\frac{1}{r}$ term in the large r expansion of a_{\pm} . By differentiating (71) at large r we find the large r relation $b'_{n+1} = -\frac{i}{2}(r^2 b'_n)' + \dots$. From (69) together with the expressions (41) we find that $b'_0 = -(B \pm i\rho/\tau)^2 \frac{1}{r^5} + \dots$. Together, this implies that we first get a $\frac{1}{r}$ contribution at order b_3 , which behaves for large r as

$$b_3 = \text{const} - \frac{3i(B \pm i\rho/\tau)^2}{4r} + \dots \quad (72)$$

We then read off the large ω behavior of the conductivity as

$$\sigma_{\pm} = \left(1 - \frac{3}{4} \frac{(B \pm i\rho/\tau)^2}{\omega^4} + \dots \right) \tau. \quad (73)$$

This result is completely universal, in that it is independent of the precise forms of the original coefficient functions U and V . From familiar UV/IR reasoning it is not surprising that the leading high frequency behavior of the conductivity only uses the asymptotic AdS behavior of the geometry, but here we see that this is also true of the subleading behavior. We have checked that (73) indeed matches on to our numerical results (presented in the next section) at large ω to excellent accuracy.

The asymptotic result for the conductivity is temperature independent, since the factors of r_+ all canceled out. This suggests that we should be able to understand the subleading term as a property of correlation functions in the zero temperature theory. We can consider this problem from the point of view of the boundary theory (see also [32, 33] for related discussion). The conductivity is related to the retarded current-current correlator according to the Kubo formula:

$$\sigma_{ij}(\omega) = \frac{i}{\omega} C_{ij}(\omega, 0), \quad (74)$$

with

$$C_{ij}(\omega, q) = \int d^3x e^{-i\omega t + iqx} \langle [J_i(t, x), J_j(0)] \rangle , \quad (75)$$

and where the expectation value is calculated in thermal equilibrium at temperature T . Since we are considering a spatially homogenous electric field we set $q = 0$.

Now, J_i is an operator of scale dimension 2, and so $C_{ij}(\omega)$ has scale dimension 1. At $T = B = \rho = 0$ scale invariance thus fixes $C_{ij}(\omega) \sim \omega$, and hence $\sigma_{ij}(\omega) \sim \omega^0$, which is just the usual statement that conductivity is dimensionless in $D = 2 + 1$.

We now break the scale invariance by turning on nonzero temperature and magnetic field, which have scale dimensions $\Delta_T = 1$, $\Delta_B = 2$. We are keeping $\rho = 0$ for simplicity. At some order, the large ω expansion of C_{ij} will involve both scales, but we can take as an *ansatz* that the first subleading term is T independent. Focussing on σ_{xx} , parity forces B to appear in even powers, and hence the allowed subleading behavior corresponds to

$$\sigma_{xx} \sim \omega^0 + \# \frac{B^2}{\omega^4} + \dots \quad (76)$$

Computing the coefficient of the subleading term requires knowledge of a four-point function evaluated at the fixed point, but the fact that the form of (76) agrees with our previous result (73) seems to justify the assumption of temperature independence at this order.

4 AC conductivity of finite temperature critical point

We now turn to the computation of the conductivity for generic B , ρ , and ω . To keep the numerics tractable we will only consider the critical point, which corresponds to setting $f(r) = 1$, and hence τ is a constant. For definiteness, we also focus on the particular example of the D3-D7 system reviewed in section (2.1). For this case, the problem to be solved is summarized as follows. We need to solve the equation (45),

$$\mathcal{C} \partial_r^2 a_{\pm} + (\mathcal{C}' - 2i\omega\mathcal{A}) \partial_r a_{\pm} - i\omega(\mathcal{A}' \mp i\mathcal{B}') a_{\pm} = 0 , \quad (77)$$

where the coefficient functions are given in (41) with

$$f(r) = 1 , \quad U = \frac{r^2}{R^2} - \frac{r_+^4}{R^2 r^2} , \quad V = \frac{r^2}{R^2} . \quad (78)$$

We look for a solution with asymptotic behavior

$$a_{\pm} = a_{\pm}^{(0)} + \frac{R^2}{r} a_{\pm}^{(1)} + \dots \quad (79)$$

and then read off the conductivity from

$$\sigma_{\pm}(\omega) = \left(1 - i \frac{a_{\pm}^{(1)}}{\omega a_{\pm}^{(0)}} \right) \tau . \quad (80)$$

We can do some rescalings to simplify. We first set $R = 1$, as can obviously be done by a rescaling of r . To scale out r_+ we first introduce

$$x = r/r_+ \quad (81)$$

so that the horizon is at $x = 1$. Also define

$$\hat{B} = \frac{B}{r_+^2}, \quad \hat{\rho} = \frac{\rho}{\tau r_+^2}, \quad \hat{\omega} = \frac{\omega}{r_+}, \quad \hat{a}_\pm = r_+ a_\pm. \quad (82)$$

We can then write

$$\mathcal{A} = \frac{x^2 \sqrt{x^4 + \hat{B}^2 + \hat{\rho}^2}}{x^4 + \hat{B}^2}, \quad \mathcal{B} = \frac{\hat{B} \hat{\rho}}{x^4 + \hat{B}^2}, \quad \mathcal{C} = r_+^2 (x^4 - 1) \frac{\sqrt{x^4 + \hat{B}^2 + \hat{\rho}^2}}{x^4 + \hat{B}^2} \equiv r_+^2 \hat{\mathcal{C}} \quad (83)$$

and our equation (77) becomes

$$\hat{\mathcal{C}} \hat{a}_\pm'' + (\hat{\mathcal{C}}' - 2i\hat{\omega}\mathcal{A}) \hat{a}_\pm' - i\hat{\omega}(\mathcal{A}' \mp i\mathcal{B}') \hat{a}_\pm = 0 \quad (84)$$

where now $' = \frac{d}{dx}$.

The asymptotic behavior is now

$$\hat{a}_\pm = \hat{a}_\pm^{(0)} + \frac{1}{x} \hat{a}_\pm^{(1)} + \dots \quad (85)$$

and the conductivity is

$$\sigma_\pm(\hat{\omega}) = \left(1 - i \frac{\hat{a}_\pm^{(1)}}{\hat{\omega} \hat{a}_\pm^{(0)}} \right) \tau. \quad (86)$$

Given the above, we will compute the conductivity as a function of the rescaled frequency $\hat{\omega}$ and the rescaled parameters $\hat{\rho}$ and \hat{B} .

4.1 Numerical results

We are now ready to numerically integrate (84). We demand that \hat{a}_\pm is a smooth function at the horizon $x = 1$, which we recall is actually a statement about smoothness at the *future* horizon, since Eddington-Finkelstein coordinates do not cover the past horizon. Since only the ratio $\frac{\hat{a}_\pm^{(1)}}{\hat{\omega} \hat{a}_\pm^{(0)}}$ appears in the conductivity, we are free to choose the horizon boundary condition $\hat{a}_\pm(1) = 1$.

If we evaluate (84) at the horizon, where $\mathcal{C}(1) = 0$ and $\mathcal{C}'(1) = 4\mathcal{A}(1)$, we can solve for the initial value of $\hat{a}_\pm'(1)$ as

$$\hat{a}_\pm'(1) = \frac{i\hat{\omega}(\mathcal{A}'(1) \mp i\mathcal{B}'(1))}{(4 - 2i\hat{\omega})\mathcal{A}(1)}. \quad (87)$$

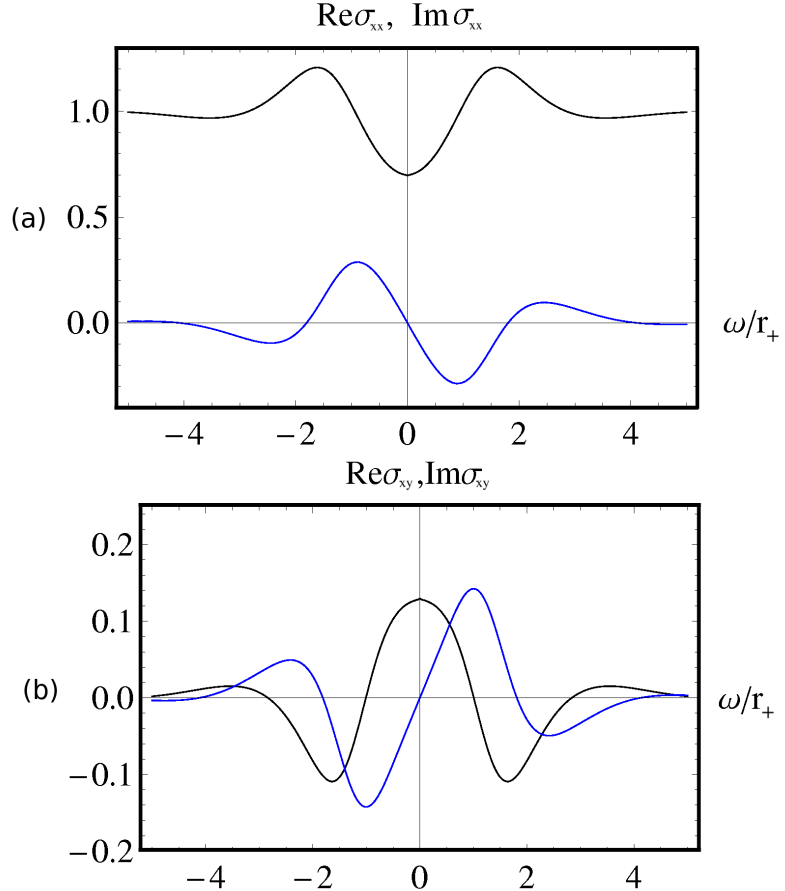


Figure 5: Real and imaginary parts of the (a) longitudinal and (b) Hall conductivity, plotted over a range of negative to positive frequencies to illustrate symmetry and antisymmetry. In (a), the top (black) curve is the real part and bottom (blue) curve is the imaginary part of the longitudinal conductivity σ_{xx} , for parameter values $\hat{\rho} = 0, \hat{B} = 1, \tau = 1$. The value at $\omega = 0$ corresponds to the DC conductivity $\sigma_{xx} = 1/\sqrt{1 + \hat{B}^2}$, a special case of (56). In (b), the symmetric (black) curve is the real part and the antisymmetric (blue) curve is the imaginary part of the Hall conductivity σ_{xy} , for parameter values $\hat{\rho} = 0.25, \hat{B} = 1, \tau = 1$.

Our initial conditions at the horizon are thus fixed, and we can proceed to integrate outward in a straightforward fashion.

Figure 5 illustrates the symmetry properties of the conductivities. The real part of the longitudinal and Hall conductivity is symmetric under the reflection $\omega \rightarrow -\omega$, while the imaginary parts are antisymmetric. The figure shows the longitudinal conductivity σ_{xx} at $\hat{\rho} = 0, \hat{B} = 1$. A non-zero Hall conductivity requires $\hat{\rho} \neq 0$, the figure shows a plot of σ_{xy} for $\hat{\rho} = 0.25, \hat{B} = 1$. The third parameter, the Born-Infeld action coefficient τ corresponds to rescaling of the y -axis, and determines the

asymptotic value of $\text{Re}\sigma_{xx}$. Here we have set $\tau = 1$.

As the parameter $\hat{\rho}$ is turned on, the plots develop more structure. Figure 6 depicts plots of σ_{xx} for various values of the parameters $\hat{\rho}, \hat{B}$. Figure 6 (a) depicts the effect of keeping $\hat{\rho}$ fixed while \hat{B} is varied: the peaks of the curves move towards higher frequencies, as would be expected if they are associated with a cyclotron frequency. Figure 6 (b) illustrates the opposite choice, keeping \hat{B} fixed while $\hat{\rho}$ is varied. The (Drude) peak of the conductivity grows when charge density increases, as expected. Figures 6 (c) and (d) focus on the real part of the longitudinal conductivity, showing the effect of larger charger densities for two fixed values of the magnetic field. When the magnetic field is turned on, (d) illustrates how the Drude peak grows but also moves to lower frequencies as the charge density increases. In all figures the real part of σ_{xx} asymptotes to one, because we fixed $\tau = 1$.

For the Hall conductivity, the plots are qualitatively similar, except that now the high-frequency limit gives zero. Figure 7 shows two series of plots for the real and imaginary part of σ_{xy} . The figure (a) shows the effect of varying \hat{B} while $\hat{\rho}$ is fixed, and (b) depicts the opposite case.

In Fig. 2 we give a comparison with the results of Sachdev. Note that many of the plots in Figures 6 and 7 are qualitatively similar to Figure 2 of [13]. This suggests that the first peak may be determined by a cyclotron resonance, which in turn depends on kinematics [12]. However, for the agreement depicted in Fig. 2, we need to purposely choose three parameters (ρ, B, τ) in order to make the curves match up nicely. It is unexpected that we can do this, since we are comparing four different curves while only tuning three constants. The cyclotron resonance may not be sufficient to explain the more detailed agreement.

5 Conclusion

Quantum Hall critical points are a very promising arena for applying AdS/CFT methods to condensed matter physics. Here we studied the AC electrical response in a class of such critical points, and obtained a variety of analytical and numerical results. One outcome was the unexpectedly good agreement between our results and those obtained previously by Sachdev, as displayed in Fig. 2. We note that the curves match nicely despite of the utterly different computational methods. It would of course be especially interesting to compare with experimental results for AC transport in these systems, if/when these become available.

Also encouraging was the high degree of universality exhibited by our results. This was seen in both the low and high frequency regimes. In the DC limit, we found that the conductivities over the entire plateau transition just depend on the entropy density of the theory and the effective brane tension at the horizon. In the high frequency regime we found universal results for both the leading and subleading

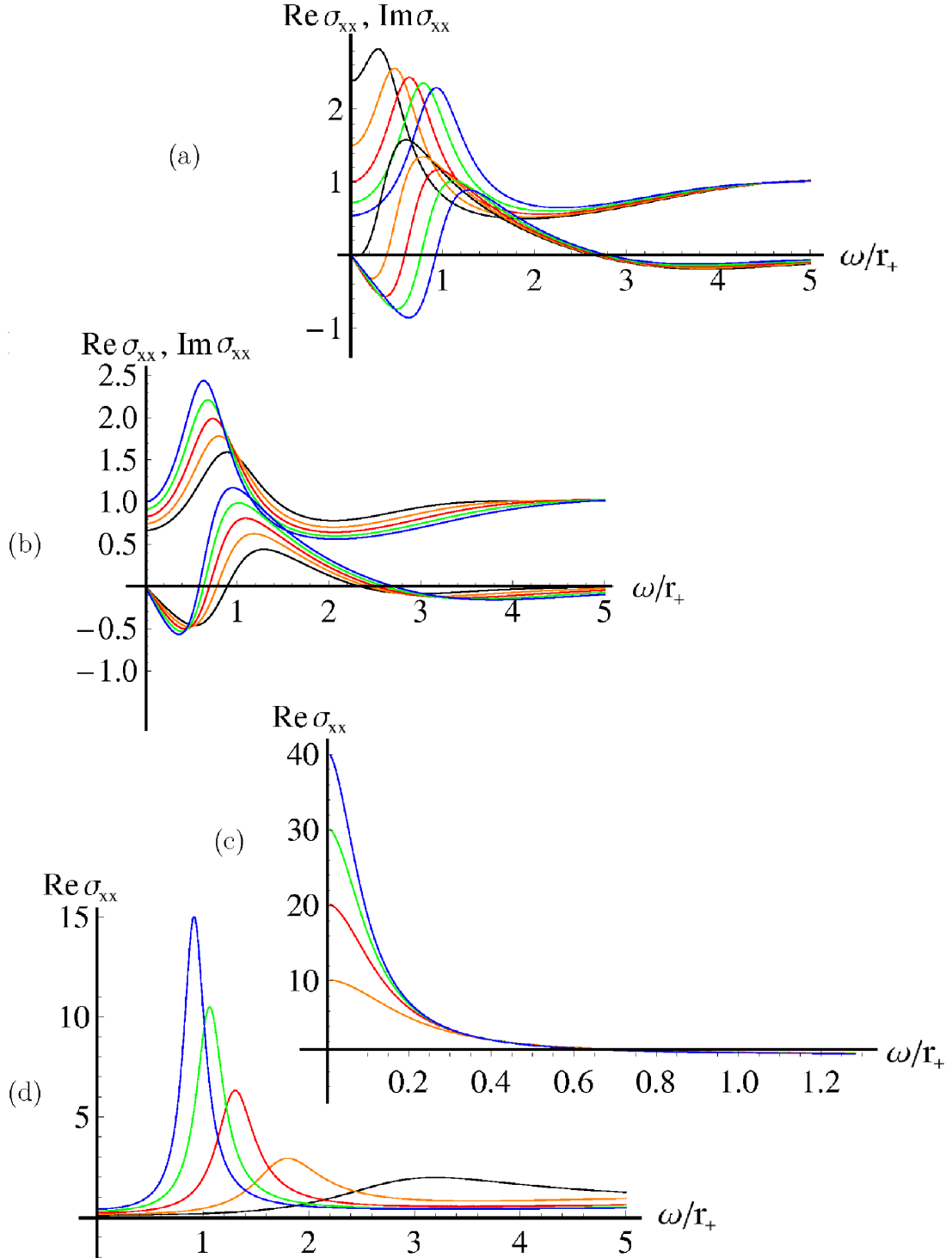


Figure 6: Real part (top curves) and imaginary part (bottom curves) of the longitudinal conductivity σ_{xx} . The x -axis is ω/r_+ . Figure (a) is for $\hat{\rho} = 4.5$, the curves represent 5 different values $\hat{B} = 1, 1.5, 2, 2.5, 3$, with colors black, orange, red, green, blue. (b) is for $\hat{B} = 2$, with $\hat{\rho} = 2.5, 3.0, 3.5, 4.0, 4.5$, (c) is for $\hat{B} = 0$, with $\hat{\rho} = 0, 10, 20, 30, 40$, (d) is for $\hat{B} = 10$, with $\hat{\rho} = 0, 10, 20, 30, 40$. The values at $\omega = 0$ correspond to the DC conductivity σ_{xx} of (56).

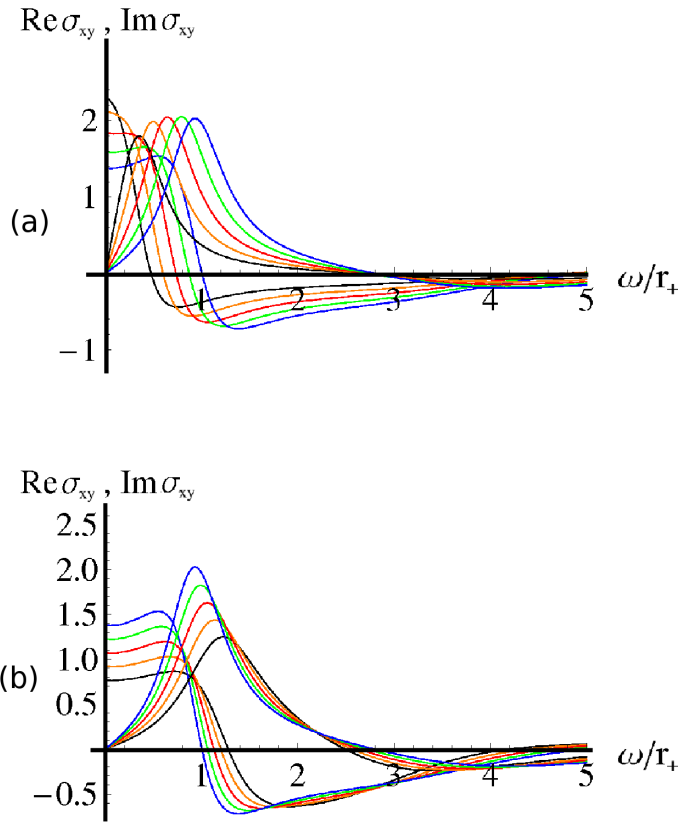


Figure 7: Real part (non-zero values at $\hat{\omega} = 0$) and imaginary part (passing through zero at $\hat{\omega} = 0$) of the Hall conductivity σ_{xy} . Figure (a) is for fixed $\hat{\rho} = 4.5$, with $\hat{B} = 1, 1.5, 2, 2.5, 3$, plot (b) is for fixed $\hat{B} = 3$, with $\hat{\rho} = 2, 2.5, 3, 3.5, 4, 4.5$.

behavior at the critical point. It is of course precisely such robust quantities that one might hope to compare successfully with real physical systems.

We have emphasized an interpretation of our critical points in terms of the quantum Hall effect, but our results can also be viewed in more general terms as modeling $2+1$ dimensional critical points with nonzero charge density and magnetic field. In this sense, our probe brane based approach is complementary to that based on using the dyonic black brane solution as a starting point [10, 11, 12, 13]. It might be informative to generalize further by combining the two sets of ingredients. In the near future we plan to study the poles in the complex frequency plane that determine the response curves, especially the role of the cyclotron resonance.

Acknowledgments We thank Josh Davis, Ari Harju, Sean Nowling, Gordon Semenoff, and Patta Yogendran for useful comments and discussions. JA has been supported in part by the Magnus Ehrnrooth foundation. EK-V has been supported in part by the the Academy of Finland grant nr. 1127482. Work of PK is supported in part by NSF grant PHY-0456200. VS-U has been supported in part by the Väisälä fund of the Finnish Academy of Science and Letters. EK-V thanks the Aspen Center for Physics for hospitality during the completion of this work.

References

- [1] S. A. Hartnoll, “Lectures on holographic methods for condensed matter physics,” arXiv:0903.3246 [hep-th].
- [2] C. P. Herzog, “Lectures on Holographic Superfluidity and Superconductivity,” arXiv:0904.1975 [hep-th].
- [3] S. Sachdev and M. Mueller, “Quantum criticality and black holes,” arXiv:0810.3005 [cond-mat.str-el].
- [4] J. L. Davis, P. Kraus and A. Shah, “Gravity Dual of a Quantum Hall Plateau Transition,” JHEP **0811**, 020 (2008) [arXiv:0809.1876 [hep-th]].
- [5] S. J. Rey, Talk given at Strings 2007 in Madrid (slides available online at <http://www.ift.uam.es/strings07/040> scientific07 contents/transparencies/rey.pdf).
- [6] S. Sachdev, “Non-zero temperature transport near fractional quantum Hall critical points,” Physical Review B 57, 7157 (1998); . [arXiv:cond-mat/9709243].
- [7] W. Chen, M. P. A. Fisher and Y. S. A. Wu, “Mott transition in an anyon gas,” Phys. Rev. B **48**, 13749 (1993) [arXiv:cond-mat/9301037].

- [8] K. Damle and S. Sachdev, “Non-zero temperature transport near quantum critical points,” *Physical Review B* **56**, 8714 (1997); . [arXiv:cond-mat/9705206].
- [9] L. P. Kadanoff and G. Baym, *Quantum Statistical mechanics*, Benjamin, NY (1962).
- [10] C. P. Herzog, P. Kovtun, S. Sachdev and D. T. Son, “Quantum critical transport, duality, and M-theory,” *Phys. Rev. D* **75**, 085020 (2007) [arXiv:hep-th/0701036].
- [11] S. A. Hartnoll and P. Kovtun, “Hall conductivity from dyonic black holes,” *Phys. Rev. D* **76**, 066001 (2007) [arXiv:0704.1160 [hep-th]].
- [12] S. A. Hartnoll, P. K. Kovtun, M. Muller and S. Sachdev, “Theory of the Nernst effect near quantum phase transitions in condensed matter, and in dyonic black holes,” *Phys. Rev. B* **76**, 144502 (2007) [arXiv:0706.3215 [cond-mat.str-el]].
- [13] S. A. Hartnoll and C. P. Herzog, “Ohm’s Law at strong coupling: S duality and the cyclotron resonance,” *Phys. Rev. D* **76**, 106012 (2007) [arXiv:0706.3228 [hep-th]].
- [14] R. C. Myers and M. C. Wapler, “Transport Properties of Holographic Defects,” *JHEP* **0812**, 115 (2008) [arXiv:0811.0480 [hep-th]].
- [15] J. H. Brodie, L. Susskind and N. Toumbas, “How Bob Laughlin tamed the giant graviton from Taub-NUT space,” *JHEP* **0102**, 003 (2001) [arXiv:hep-th/0010105].
- [16] O. Bergman, Y. Okawa and J. H. Brodie, “The stringy quantum Hall fluid,” *JHEP* **0111**, 019 (2001) [arXiv:hep-th/0107178].
- [17] S. Hellerman and L. Susskind, “Realizing the quantum Hall system in string theory,” arXiv:hep-th/0107200.
- [18] E. Keski-Vakkuri and P. Kraus, “Quantum Hall Effect in AdS/CFT,” *JHEP* **0809**, 130 (2008) [arXiv:0805.4643 [hep-th]].
- [19] S. A. Hartnoll, C. P. Herzog and G. T. Horowitz, “Building a Holographic Superconductor,” *Phys. Rev. Lett.* **101**, 031601 (2008) [arXiv:0803.3295 [hep-th]].
- [20] M. Fujita, W. Li, S. Ryu and T. Takayanagi, “Fractional Quantum Hall Effect via Holography: Chern-Simons, Edge States, and Hierarchy,” arXiv:0901.0924 [hep-th].
- [21] Y. Hikida, W. Li and T. Takayanagi, “ABJM with Flavors and FQHE,” arXiv:0903.2194 [hep-th].

- [22] O. Aharony, O. Bergman, D. L. Jafferis and J. Maldacena, “N=6 superconformal Chern-Simons-matter theories, M2-branes and their gravity duals,” *JHEP* **0810**, 091 (2008) [arXiv:0806.1218 [hep-th]].
- [23] A.W.W. Ludwig, M.P.A. Fisher, R. Shankar, G. Grinstein, “Integer quantum Hall transition: An alternative approach and exact results” *Phys. Rev. B* **50**, 7526 (1994).
- [24] A. Karch and E. Katz, “Adding flavor to AdS/CFT,” *JHEP* **0206**, 043 (2002) [arXiv:hep-th/0205236].
- [25] J. Erdmenger, N. Evans, I. Kirsch and E. Threlfall, “Mesons in Gauge/Gravity Duals - A Review,” *Eur. Phys. J. A* **35**, 81 (2008) [arXiv:0711.4467 [hep-th]].
- [26] S. Hohenegger and I. Kirsch, “A note on the holography of Chern-Simons matter theories with flavour,” arXiv:0903.1730 [hep-th].
- [27] D. Gaiotto and D. L. Jafferis, “Notes on adding D6 branes wrapping RP3 in AdS4 x CP3,” arXiv:0903.2175 [hep-th].
- [28] S. Bhattacharyya, V. E. Hubeny, S. Minwalla and M. Rangamani, “Nonlinear Fluid Dynamics from Gravity,” *JHEP* **0802**, 045 (2008) [arXiv:0712.2456 [hep-th]].
- [29] D. T. Son and A. O. Starinets, “Minkowski-space correlators in AdS/CFT correspondence: Recipe and applications,” *JHEP* **0209**, 042 (2002) [arXiv:hep-th/0205051].
- [30] A. O’ Bannon, “Hall Conductivity of Flavor Fields from AdS/CFT,” *Phys. Rev. D* **76**, 086007 (2007) [arXiv:0708.1994 [hep-th]].
- [31] S. Sachdev, “Quantum Phase Transitions”, Cambridge University Press, (2001)
- [32] R. C. Myers and A. Sinha, “The fast life of holographic mesons,” *JHEP* **0806**, 052 (2008) [arXiv:0804.2168 [hep-th]].
- [33] R. C. Myers, A. O. Starinets and R. M. Thomson, “Holographic spectral functions and diffusion constants for fundamental matter,” *JHEP* **0711**, 091 (2007) [arXiv:0706.0162 [hep-th]].